Experimental Heat Transfer: A Journal of Thermal Energy Generation, Transport, Storage, and Conversion
Publication details, including instructions for authors and subscription information:
http://www.tandfonline.com/loi/ueht20

Modeling of Thermal Conductivity of Concrete with Vermiculite Using by Artificial Neural Networks Approaches

O. Gencel [a b], F. Koksal [c], M. Sahin [c], M. Y. Durgun [a], H. E. Hagg Lobland [b] & W. Brostow [b]

[a] Department of Civil Engineering, Faculty of Engineering, Bartin University, Bartin, Turkey

[b] Laboratory of Advanced Polymers and Optimized Materials (LAPOM), Department of Materials Science and Engineering and Center for Advanced Research and Technology (CART), University of North Texas, Denton, Texas, USA

[c] Department of Civil Engineering, Faculty of Engineering and Architecture, Bozok University, Yozgat, Turkey

Accepted author version posted online: 30 Nov 2012.Published online: 17 May 2013.

To cite this article: O. Gencel, F. Koksal, M. Sahin, M. Y. Durgun, H. E. Hagg Lobland & W. Brostow (2013): Modeling of Thermal Conductivity of Concrete with Vermiculite Using by Artificial Neural Networks Approaches, Experimental Heat Transfer: A Journal of Thermal Energy Generation, Transport, Storage, and Conversion, 26:4, 360-383

To link to this article: http://dx.doi.org/10.1080/08916152.2012.669810

Experimental Heat Transfer, 26:360–383, 2013

ISSN: 0891-6152 print/1521-0480 online
DOI: 10.1080/08916152.2012.669810

Taylor & Francis
Taylor & Francis Group

MODELING OF THERMAL CONDUCTIVITY OF CONCRETE WITH VERMICULITE USING BY ARTIFICIAL NEURAL NETWORKS APPROACHES

O. Gencel,[1,2] F. Koksal,[3] M. Sahin,[3] M. Y. Durgun,[1] H. E. Hagg Lobland,[2] and W. Brostow[2]

[1]*Department of Civil Engineering, Faculty of Engineering, Bartin University, Bartin, Turkey*

[2]*Laboratory of Advanced Polymers and Optimized Materials (LAPOM), Department of Materials Science and Engineering and Center for Advanced Research and Technology (CART), University of North Texas, Denton Texas, USA*

[3]*Department of Civil Engineering, Faculty of Engineering and Architecture, Bozok University, Yozgat, Turkey*

In this article, the thermal conductivity of concrete with vermiculite is determined and also predicted by using artificial neural networks approaches, namely the radial basis neural network and multi-layer perceptron. In these models, 20 datasets were used. For the training set, 12 datasets (60%) were randomly selected, and the residual datasets (8 datasets, 40%) were selected as the test set. The root mean square error, the mean absolute error, and determination coefficient statistics are used as evaluation criteria of the models, and the experimental results are compared with these models. It is found that the radial basis neural network model is superior to the other models.

Keywords artificial neural networks, concrete, thermal conductivity, vermiculite, numerical simulation

INTRODUCTION

Economical and environmental constraints are bound to increase in the coming years, and one effect of this on the construction industry will be the need to obtain more energy-efficient buildings and construction materials [1]. Buildings are considered as open systems, and in that sense, they interact with the environment. Part of this interaction includes thermal energy transmission carried out by the heat transfer mechanisms of conduction, convection, and radiation. Heat transfer toward the inside of a building occurs through opaque (roofs and walls) and semitransparent (glass windows, skylights) materials [2]. Energy use in buildings is a significant factor in the world's overall energy consumption and a major contributor to greenhouse gases. Approximately 25–30% of the total energy currently consumed in the world is used in buildings. About 80% of the energy consumed in commercial and residential buildings is used for space heating and

Received 4 August 2011; accepted 12 January 2012.
Address correspondence to Dr. Osman Gencel, Department of Civil Engineering, Faculty of Engineering, Bartin University, 74100 Bartin, Turkey. E-mail: osmangencel@gmail.com

NOMENCLATURE

ANN	artificial neural network	MLP	multi-layer perceptron
ARE	absolute relative error	MLR	multiple linear regression
ASTM	American Society for Testing and Materials	MNLR	multiple non-linear regression
		r	scalar radius
c	center for RBNN	RBNN	radial-based neural networks
CEM	cement type	r_j	Euclidean length
C-S-H	calcium silica hydrate	RMSE	root mean square error
EN	European norm	SEM	scanning electron microscope
h	hour	TC	thermal conductivity
HM	Hessian matrix	V/C	vermiculite-to-cement ratio
kg	kilogram	W	watt
LM	Levenberg–Marquardt	$x_{\max}$	maximum of the training data
m	meter	$x_{\min}$	minimum of the training data
MAE	mean absolute error	ϕ	activation functions used for RBNN
Mg	magnesium	ξ	metric for RBNN
min	minute	$^{\circ}$C	centigrade
mK	meter Kelvin		

cooling. An important way of achieving better energy efficiency in buildings is to improve their thermal insulation properties. Reduction of the heat loss in buildings decreases the consumption of energy and, thus, reduces the cost of heating and cooling [3, 4].

Enhanced thermal protection is a therefore a prerequisite to construct or rehabilitate buildings to reach a reasonable energy consumption, satisfactory thermal comfort conditions, and low operational costs. Energy saving can be obtained by insulation since a significant part of heat losses or heat gains occurs through walls and ceilings [5–7]. In recent years, in countries of mild climate, more attention has been given than before to reducing energy consumption while maintaining or improving comfort conditions in buildings. To this end, effort has been concentrated on improving the efficiency of heating appliances and the thermal insulation of buildings. So, heat transfer with the maximum possible efficiency by using adequate materials is as important as avoiding heat losses. The knowledge of a material's physical properties is very important in all engineering projects. Energy conservation is an important part of any national energy strategy, and energy conservation in developing countries with inadequate resources is even more important [8–15]. An analysis of conduction heat transfer through structure is of great importance in civil engineering problems, such as heat flow into a building in energy-efficient building design, thermal loading of structures due to diurnal variations of temperature, planning and design of building for thermal comfort, design of radiation shields in nuclear power stations, analysis of bridge deck and other exposed structures for solar thermal loading, etc. The knowledge of thermal conductivity (TC) and other thermal transport properties of construction materials involved in the process of heat transfer is essential in predicting the temperature profile and heat flow through the material. The TC of concrete—one of the most commonly used construction materials—draws importance [16, 17]. Concrete of low TC is useful for the thermal isolation of buildings [18].

Concrete is a composite material, and since approximately 75% of the concrete volume is occupied by aggregate, the properties of aggregate greatly affect performance of concrete. Several properties of aggregate, such as chemical and mineral composition,

shape, roughness, specific gravity, hardness, strength, and pore structure, depend on the properties of the parent rock [19]. The use of lightweight and porous aggregates as a constituent of concrete enables production of lightweight concrete. Due to its higher porosity, lightweight concrete is a suitable material for thermal insulation of structures [1]. Parameters affecting the TC of concrete are presented in Figure 1.

Lightweight concrete is destined to become a dominant construction material in the world because of its lower density and unique soundproofing and thermal properties. Lightweight concrete has a density that is dependent on the size and number of pores within the sample [20]. Lightweight concrete has many useful applications despite its lower strength as compared to normal concrete. For instance, concrete lightweight blocks are widely used in the construction of claddings and load and non-load bearing walls and partitions. In countries with extreme hot or cold climates, lightweight concrete blocks possessing low TCs also serve as a thermal insulation material, which reduces energy consumption by reducing the dependence on electricity for air conditioning or heating [21]. Also, lightweight concrete may be used in floor fills, roof decks, sound barriers, insulative fill around fireplaces, and other non-structural applications. Lightweight concrete is typically made by incorporating a lightweight aggregate [20], which is generally classified into two groups: (1) natural (pumice stone, diatomite, volcanic slag, etc.) and (2) artificial (perlite, schist, expanded clay or vermiculate, slate, etc.) [22].

Heat transfer in concrete is complicated. In order to facilitate a better understanding of conduction phenomena, one must subdivide the concrete into its constituents and facets and study the heat transfer through each of these to understand the relative importance and contribution of the component heat transfer to the overall thermal behavior of the concrete. A review of earlier investigations reveals that the type of aggregate, porosity, and moisture content have the most influence on TCs of concrete, while the cement hydrates exert a smaller influence as their TC varies less. Thus, the TC of aggregates

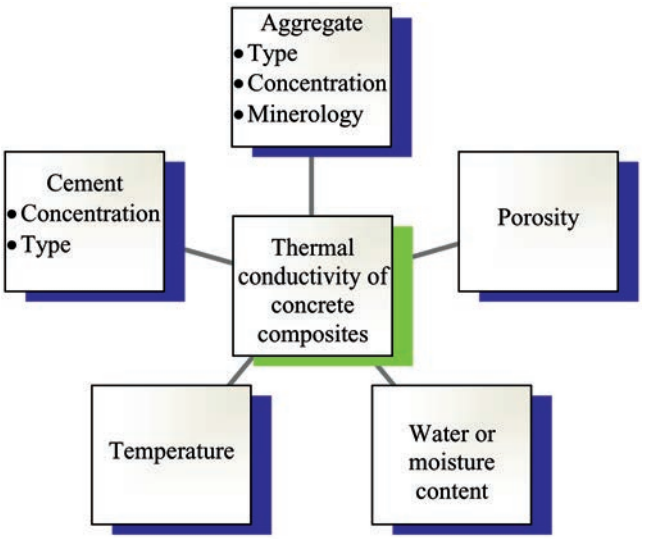

Figure 1. Parameters affecting TC of cement-based composites. (color figure available online)

primarily determines the insulating quality of the concrete. The TC of rocks, commonly used as aggregates in concrete, ranges from 1.163 to 8:6 W/mK. Aggregates with less TC produce the less conductive concrete, whereas the more conductive aggregates produce more conductive concrete. Thus, aggregate type can cause nearly twice an increase in the TC of concrete. One way of resolving the problem of energy saving is the use of high-quality heat-insulating materials. The materials mostly used are based on vermiculite and diatomite [16].

Vermiculite is a mica-type mineral usually formed by hydrothermal decompositions, such as biotite and phologopite [23]. It has a layer structure, and the interlayer contains water molecules and exchangeable cations, mainly Mg^{2+} [24]. Expanded vermiculite is obtained by calcinating the raw vermiculite ore or its concentrate. Vermiculite expands as much as 8 to 30 times its original volumes when heated above 300°C, typically up to 870°C–1,090°C. The interlayer and structural water is converted to steam, and thus, an efficient heat-insulating material with a density of 60–150 kg/m^3 results [25, 26]. It can be used at temperatures from −240°C to +1,100°C. After expansion, it exhibits a number of advantageous properties, such as low bulk density, low heat conductivity (0.04–0.12 W/mK), and a relatively high melting point (1,240°C–1,430°C) [27]. It also becomes chemically inert, durable, and environmentally safe. The properties of expanded vermiculite depends on the quality of the raw material, its fractional composition, heating rate, holding time at a maximum temperature, cooling rate, moisture content, and the heating method employed. The particles of expanded vermiculite are generally viewed as slender plates separated by a thin air gap. Their properties, such as shape, color, luster, and grain composition, are closely related to the original raw material. Fired, expanded vermiculite has been used for various industrial and agricultural applications, including gaskets for high-temperature sealing, such as in catalytic converters; insulation and fire retardants; various construction products; potting soils; soil conditioners; carriers for fertilizers; insecticides and herbicides; various livestock applications; and ammonia filtering in aquaculture [28].

For years, research has been carried out using various methods in order to anticipate the concrete properties. Studying correlation between the thermal property and the characteristic parameters, e.g., the composition of those materials and their service conditions, is of importance for designing the proper composites in order to satisfy various requirements. The development of a model based on existing experimental data becomes necessary to predict material properties. It may significantly further reduce experimental work in the design of composite materials. Simulation of material properties generally involves the development of a mathematical model derived from experimental data; it is helpful in the optimization of such composite materials as concrete [29]. Therefore, artificial neural networks (ANNs) have been introduced into this field in recent years and successfully applied in a number of diverse fields, since the model approaches seem to have good potential to save time and cut expenses in solving various engineering problems. However, no study has been carried out to utilize the application of the RBNN and MLP computing techniques in modeling the TC of concrete. The purpose of this study is to estimate experimental values of TCs of concrete proportioned with different cement content and vermiculate content under different elevated temperatures.

The ANN has an ability to learn complex and non-linear relationships that are difficult to model with conventional techniques. Thus, the ANN has been used successfully for prediction of concrete properties. Optimization of concrete mix proportioning using

ANNs was studied in [30–33]. The applicability of neural networks for the prediction of workability and slump of concrete was investigated in [34–37]. Hardened properties of concrete, such as concrete strength, ultrasonic pulse velocity, elastic modulus, mechanical behavior at high temperature, were predicted in [38–43].

As based on an extensive literature survey, and according to the best knowledge of the authors, there is no published work indicating the input–output mapping capability of the ANN technique in modeling the TCs of concrete. The aim of this article is to investigate the accuracy of RBNN and MLP approaches in modeling TCs of concrete. The performances of the RBNN and MLP models are compared with those of multiple nonlinear regression (MNLR) and multiple linear regression (MLR) models. The presented article is the first application for modeling TCs of concrete using ANN models.

This paper is organized as follows. The next section introduces the experimental studies, followed by the methodologies and the applications of model approaches in the following section. The penultimate section presents experimental test results and the results of model approaches, with the last section giving conclusions.

MATERIALS AND METHODS

Experimental Studies

Cement type (CEM) I 42.5R portland cement was used as a binder; chemical and physical properties of the cement are given in Table 1. It complies with the requirement of European Standards European norm (EN) 197-1 [44]. Expanded vermiculite was obtained by annealing raw vermiculite at about 600°C for 10 sec. Raw vermiculite is procured from the Demircilik vermiculite deposit in Yıldızeli, Sivas, Turkey. The chemical and physical properties of expanded vermiculite are given in Table 2.

For the mixing procedure, cement and water were first mixed together for 1 min in a mixer; dried expanded vermiculite is then added to the cement slurry and mixed again for 3 min to get a homogenous structure. Before producing specimens, trial batches

Table 1. Chemical and physical properties of cement

Composition	Percent
Chemical properties	
SiO_2	19.4
Al_2O_3	5.6
Fe_2O_3	2.4
CaO	63.1
MgO	2.6
SO_3	2.9
Na_2O	0.8
K_2O	1
CI	0.01
Insoluble material	3.3
Loss on ignition	3.3
Physical properties	
Specific gravity (g/cm^3)	3.06
Specific surface (cm^2/g)	3,940

Table 2. Properties of expanded vermiculite

Composition	Percent
Chemical properties	
SiO_2	34.1
Al_2O_3	17.2
K_2O	4.5
CaO	6.4
MgO	16.3
Fe_2O_3	14.7
pH (in water)	6.1
Others	0.7
Physical properties	
Color	Silver
Shape	Accordion-shaped granule
Water-holding capacity	240% (by weight)
Cation-exchange capacity	90 meg/100 gr.
TC value	0.063 watt/m/°C
Sintering temperature	1,170°C
Combustibility	Non-combustible
Specific heat	0.22 Kcal/Kg°C
Bulk density	140 kg/m^3
Particle size distribution	
Sieve size (mm)	Passing (%)
8	100
4	53.3
2	14.1
1	3.8
0.5	2.4
0.25	1.7
0.125	1

were made to determine the water content of each mix at which slump would be zero. Four different expanded vermiculite to binder ratios of 3, 4, 5, and 6, by volume, were used; test temperatures were 20°C, 300°C, 600°C, 900°C, and 1,100°C. For each testing temperature, 4 series of cement-based lightweight composite specimens with a different expanded vermiculite-to-binder ratio were produced, and in total, 20 concrete series were tested in this experimental research. The mix compositions of each series are given in Table 3. For the mix code of series, VC3, VC4, VC5, and VC6 refer to vermiculite-to-binder ratios of 3, 4, 5, and 6 by volume, respectively.

The prepared fresh cement-based composites were cast in standard cylinder (150 mm in diameter and 300 mm high) and cube (with an edge of 150 mm) molds, in two layers, each layer being compacted by its self-weight on the shaker for 20 sec. All specimens were kept in the molds for 24 h at room temperature of about 20°C and then demoulded; after demolding, all specimens were cured in water at 23 ± 2°C for 27 days. Tests of unit weight, apparent porosity, and water absorption were performed on the specimens at the end of 28 days according to Archimedes principle.

Table 3. Mix proportions of concrete series

Mix code	V/C (by volume)	Cement (kg/m^3)	Vermiculite (kg/m^3)	Water (kg/m^3)
VC3	3	750	149	471
VC4	4	636	180	541
VC5	5	522	187	566
VC6	6	422	192	580

A compressive strength test carried out on three cylinder specimens and the average values of the test results were reported for each testing temperatures. The compressive strength test was made in accordance with the American Society for Testing and Materials (ASTM) C39 [45]. TC tests were made on plate specimens obtained by cutting the cube specimens into pieces with dimensions of $150 \times 150 \times 25$ mm. The cutting procedure was made before exposing the specimens to high temperatures. The TCs of specimens were determined by the "hot wire method" according to ASTM C1113 [46]. This method has wide applications in determining TCs of refractory materials [47–49]. The TC of a material is the quantity of heat transmitted through a unit thickness in a direction perpendicular to a surface of unit area, due to a unit temperature gradient under given conditions. In the mathematical formulation of the method, the hot wire is assumed to be an ideal infinitely thin and long heat source, which is in an infinite surrounding material whose TC is to be determined. Applying a constant electric current through the wire, a constant amount of heat per unit time and unit length is released by the wire and propagates throughout the material.

In this method, the temperature variation with time at certain locations is measured instead of measuring heat flow. Because of being transient in nature, TC measurement by this method takes only a few minutes in contrast to the earlier methods involving steady-state conditions. For determining the morphological and mineralogical features of specimens after exposing to high temperatures, fractured surfaces of specimens exposed to test temperatures were coated with gold in a vacuum evaporator and examined using a scanning electron microscope (SEM). An electrically heated furnace was used for heating the specimens. Cylinder and plate specimens from each series were first placed in an oven and heated from room temperature (20°C) to 300°C, 600°C, 900°C, and 1,100°C at an average rate of 5°C/min. The specimens were held at the desired test temperature for approximately 6 h, and then the furnace was turned off; finally, specimens were left to cool in air until decreasing to room temperature. During the heating period, moisture in the test specimens was allowed to escape freely. Strength and TC test results of cement-based composites exposed to high temperatures were compared with the test results of unheated specimens.

Neural Networks

The ANN modeling approach is a computer methodology that attempts to simulate some important features of the human nervous system, in other words, the ability to solve problems by applying information gained from past experience to new problems or case scenarios. Analogous to a human brain, an ANN uses many simple computational elements, named artificial neurons, connected by variable weights. The ANN modeling

consists of two steps: to train and to test the network. During the training stage, the network uses the inductive-learning principle to learn from a set of examples called the training set. Test data could not be used in training [50]. Among the much different architectures, the RBNN and MLP architectures are commonly used for prediction. Programs were written and run for the RBNN and MLP models in the MATLAB environment (The MathWorks, Natick, Massachusetts, USA).

RBNNs. RBNNs were introduced into the neural network literature by Broomhead and Lowe [51]. The RBNN model is motivated by the locally tuned response observed in biological neurons. Neurons with a locally tuned response characteristic can be found in several parts of the nervous system, for example, cells in the visual cortex sensitive to bars oriented in a certain direction or other visual features within a small region of the visual field [52]. The RBNNs utilize a clustering process on the input data before presentation to the network and use different non-linear activation functions that are locally tuned to cover a region of the input space. The network structure is shown in Figure 2, and it consists of an input layer, a single hidden layer containing the same number of nodes as the cluster centers, and an output layer [53].

The basis functions in the hidden layer produce a significant non-zero response to input stimulus only when the input falls within a small localized region of the input space. Hence, this paradigm is also known as a localized receptive field network [54]. Transformation of the inputs is essential for fighting the curse of dimensionality in empirical modeling. The type of input transformation of the RBNN is the local non-linear projection using a radial fixed-shape basis function. After non-linearly squashing the multi-dimensional inputs without considering the output space, the radial basis functions play a role as regressors. Since the output layer implements a linear regressor, the only adjustable parameters are the weights of this regressor. These parameters can therefore

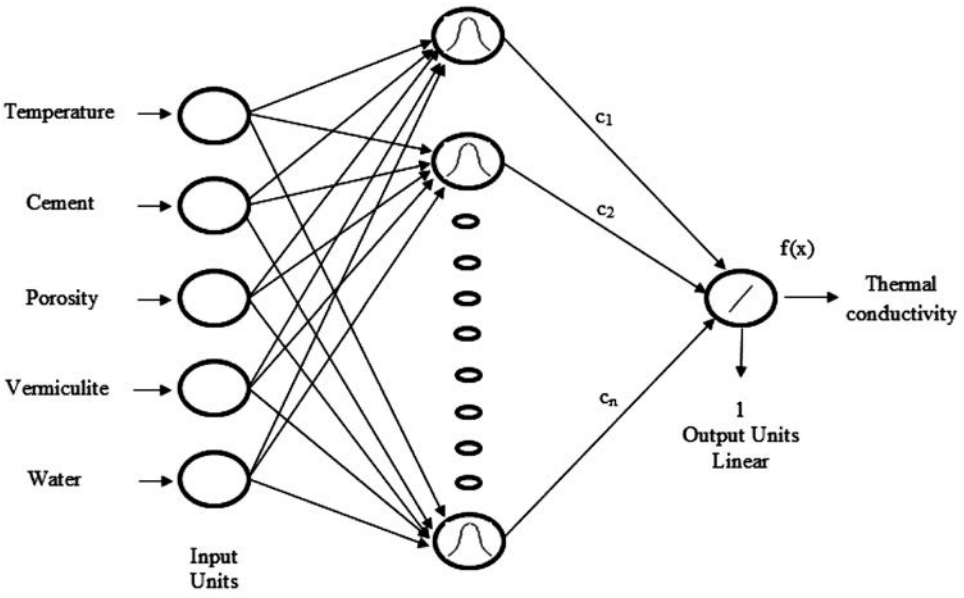

Figure 2. RBNN structure.

be determined using the linear least square method, which gives an important advantage for convergence. The most general formula for any RBNN is

$$y(x) = \varphi((x-c)^t \xi^{-1}(x-c)), \tag{1}$$

where ϕ denotes the activation functions used, c is the center, and ξ is the metric. The term $((x-c)^t \xi^{-1}(x-c))$ is the distance between x and center c in the metric defined by ξ. The metric is often Euclidean. In this case, $\xi = r^2 I$ for some scalar radius r and Eq. (1) simplifies to

$$y(x) = \varphi\left(\frac{(x-c)^t(x-c)}{r^2}\right). \tag{2}$$

According to Fausett [55], the Euclidean length is represented by r_j, which measures the radial distance between the datum vector $y = (y_1, y_2, \ldots, y_m)$ and the radial center $Y(i) = w_1, w_2, \ldots, w_{mj})$; y_i and w_{ij} are the output and weights, respectively. This can be written as

$$r_j = \|y - Y^{(j)}\| = \left[\sum_{i=1}^{m}(y_i - w_{ij})^2\right]^{1/2}. \tag{3}$$

A suitable transfer function is then applied to r_j to give

$$\phi(r_j) = \phi\left(\|y - Y^{(k)}\|\right). \tag{4}$$

Finally, the output layer ($k = 1$) receives a weighted linear combination of $\phi(r_j)$:

$$\overline{y}^{(k)} = \sum_{j=1}^{n} c_j^{(k)} \phi(r_j) = \sum_{j=1}^{n} = c_j^{(k)} \phi\left(\|y - Y^{(k)}\|\right). \tag{5}$$

This means that the RBNN can be viewed as a special case of a linear regression model. The RBNN method does not perform parameter learning as in the back-propagation networks but only performs a linear adjustment of the weights for the radial bases. This characteristic of the RBNN gives the advantage of a very fast converging time without local minima, since its error function is always convex [56, 57]. In this study, different numbers of hidden neurons and spread constants are examined for the RBNN models with a simple trial–error method.

MLPs. The network consists of layers of parallel processing elements, with each layer being fully connected to the proceeding layer by interconnection strengths or weights W. A multilayer feedforward network consists of an input layer, one or more hidden layers, and an output layer, as shown in Figure 3. Computations take place in the hidden and output layers only. Various combinations of network architecture to develop an optimum ANN model were examined. ANN (i, j, k) indicates a network architecture with i, j, and k neurons in the input, hidden, and output layers, respectively. Figure 3 illustrates a three-layer neural network consisting of layers i, j, and k, with the interconnection weights W_{ij} and W_{jk} between the layers of neurons. Initial estimated weight values are progressively corrected during a training process that compares predicted outputs with

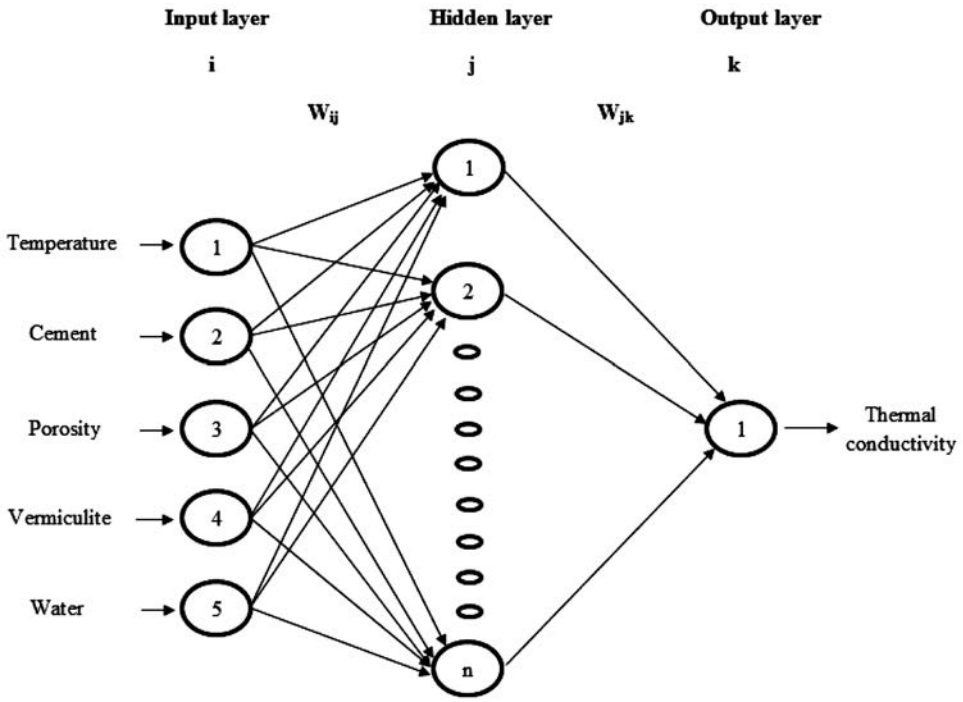

Figure 3. MLP structure.

known outputs, and back-propagates any errors (from right to left in Figure 3) to determine the appropriate weight adjustments necessary to minimize the errors. Throughout ANN simulation, the adaptive learning rates were used for the purpose of faster training speed and solving local minima problem. For each epoch, if performance decreases toward the goal, then the learning rate is increased by the factor learning increment. If performance increases, the learning rate is adjusted by the factor learning decrement. The numbers of hidden layer neurons were found using a simple trial–error method in applications. The MLPs were trained using the Levenberg–Marquardt (LM) technique, which is more powerful than the conventional gradient descent techniques [58–60]. The MLP can have more than one hidden layer; however, theoretical works have shown that a single hidden layer is sufficient for MLPs to approximate any complex non-linear function [61–63]. Therefore, in this study, one-hidden-layer MLP is used.

LM algorithm. The LM algorithm was designed to approach second-order training speed without having to compute the Hessian matrix (HM) [64, 65]. When the performance function has the form of a sum of the squares (as is typical in training feedforward networks), then the HM can be approximated as

$$HM = J^t J, \tag{6}$$

and the gradient can be computed as

$$g = J^t e, \tag{7}$$

where J is the Jacobian matrix, which contains first derivatives of the network errors with respect to the weights and biases, and e is a vector of network errors.

The LM algorithm uses this approximation to the HM in the following Newton-like update:

$$x_{k+1} = x_k - [J^t J + \mu I]^{-1} J^t e. \tag{8}$$

When the scalar μ is zero, this is just Newton's method using the approximate HM. When μ is large, this becomes gradient descent with a small step size. Newton's method is faster and more accurate near an error minimum, so the aim is to shift toward Newton's method as quickly as possible. Thus, μ is decreased after each successful step (reduction in performance function) and is increased only when a tentative step would increase the performance function. In this way, the performance function will always be reduced at each iteration of the algorithm. The application of the LM to neural network training was described in [59, 66–68].

EXPERIMENTAL RESULTS

Physical Properties

Unit weight, apparent porosity, and water absorption of unheated specimens after 28 days curing are given in Table 4. Apparent porosity and water absorption decreased with the increase of vermiculite-to-cement (V/C) ratio while unit weight was decreasing. This is a result of increasing void ratio depending on the increase of expanded vermiculite volume in the mix. Unit weights for all series specimens obtained in the range of 1,078 to 1,332 kg/m^3. On the other hand, apparent porosity changed approximately between 30 and 37%, and the change in water absorption was also between 24 and 35%.

Expanded vermiculite is a preferable lightweight material in the manufacturing of lightweight construction composites, heat-insulation and fire-resistant materials etc., because of its high pore structure and very low bulk density.

Compressive Strength

Decreases in compressive strengths were observed up to the heating temperature of 600°C for all series. However, there was a recovery in strength at the temperature of 900°C, and compressive strengths at that point were greater than the strengths at 600°C. Recovery was greater for specimens containing higher vermiculite content. This behavior may be due to re-expansion of vermiculite, resulting in filling or closing of microcracks

Table 4. Test results of unit weight, apparent porosity, and water absorption

Mix code	V/C (by volume)	Unit weight (kg/m^3)	Apparent porosity (%)	Water absorption (%)
VC3	3	1,332	29.9	24.4
VC4	4	1,183	35.8	30.7
VC5	5	1,116	36.2	31.1
VC6	6	1,078	37.4	34.6

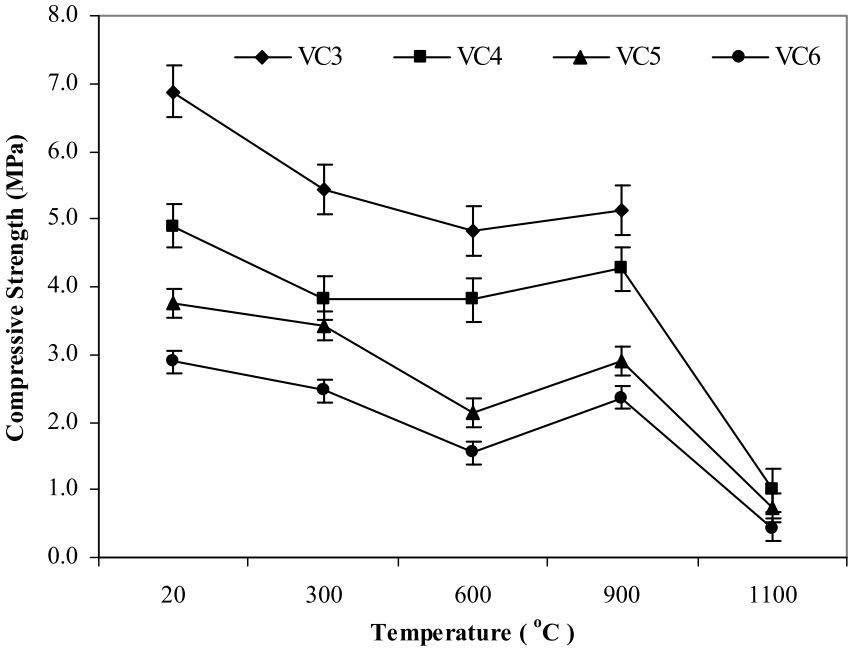

Figure 4. Residual compressive strengths at different temperatures.

and voids in microstructure. At the heating temperature of 1,100°C, a significant decrease in compressive strength was noted for each series. These results are shown in Figure 4 with error bars. Relative residual compressive strengths in comparison with the strength at 20°C after heating are also given in Figure 5. Similar results were obtained for splitting tensile strength. A failure of specimens with a high cement content (which is the lowest V/C ratio) occurred when subjected to 1,100°C; the residual strengths were not obtained.

From the residual compressive and splitting strengths point of view, it can be stated that cement-based composites, produced by using expanded vermiculite aggregate, showed a good performance up to 900°C. A considerable reduction in strength was observed above 900°C. Therefore, it can be concluded the temperature above 900°C was a critical zone for strength loss of cement-based composites produced by using expanded vermiculite.

TC

The variation of TCs of concrete with V/C ratio and heating temperature T is shown in Figure 6 with error bars. Relative residual TC in comparison with the TC at 20°C after heating is also given in Figure 7. In Figure 8, a decrease in TC is observed up to the heating temperature of 900°C for all V/C ratios. However, a slight increase is observed at the heating temperature of 1,100°C. The maximum reductions in TC of concrete occurred at 900°C for all V/C ratios. Those reductions for V/C ratios of 3, 4, 5, and 6 were 58.4, 60.1, 63.7, and 63.6, respectively, compared to the unheated control specimens. The highest values of TC of concrete is obtained for specimens produced with

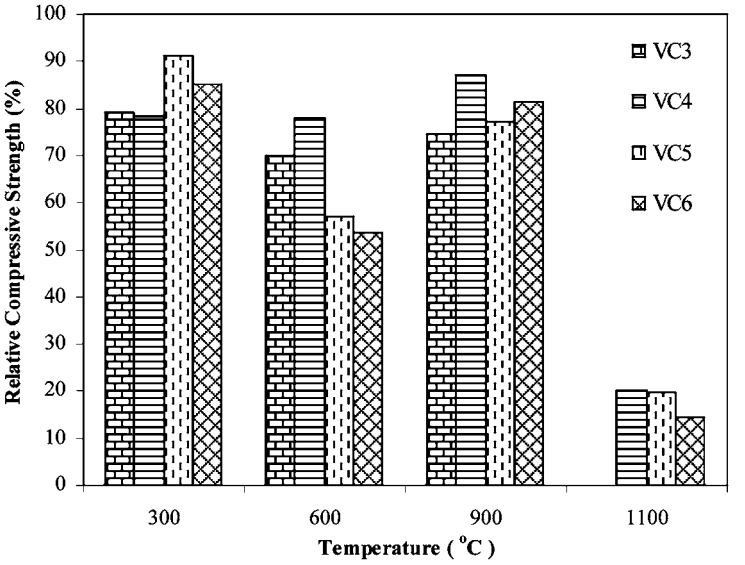

Figure 5. Relative residual compressive strengths after heating (compared to strength at 20°C).

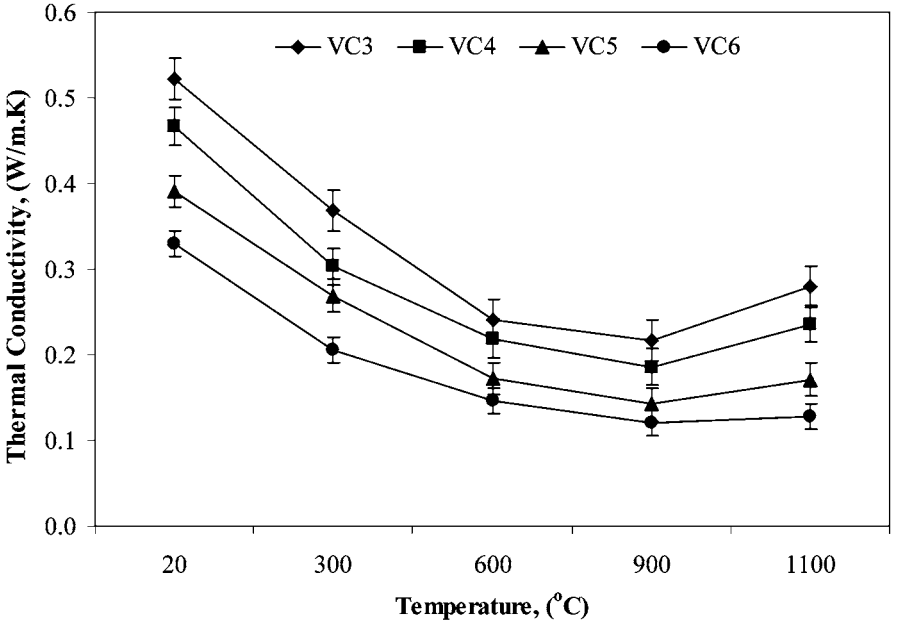

Figure 6. Residual TC at different temperatures.

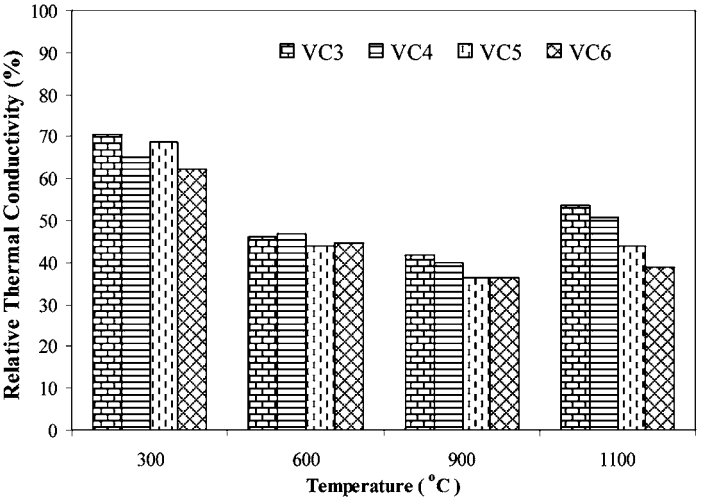

Figure 7. Relative residual TC after heating (compared to TC at 20°C).

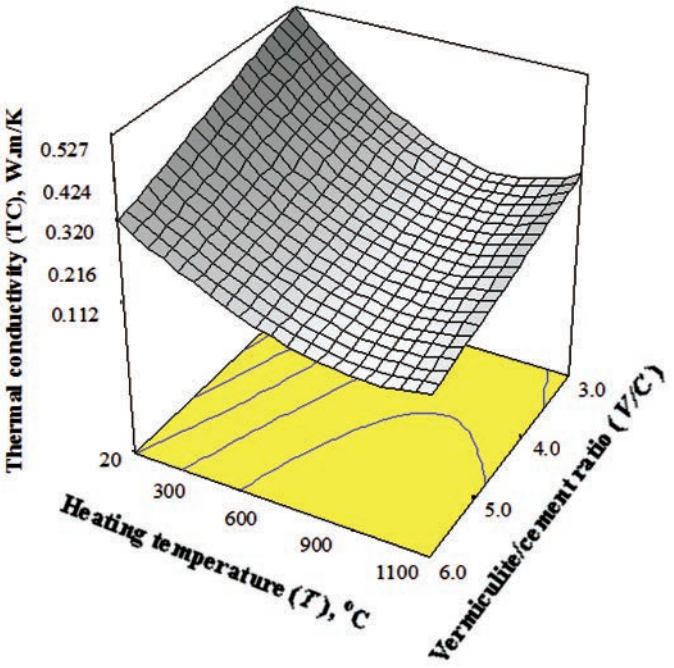

Figure 8. Response surface of TC. (color figure available online)

a V/C ratio of 6, in which cement content is high, for all heating temperatures. It can be stated that reductions were partly due to the density. Density decreased with increasing expanded vermiculite content in the mix. Additionally, Akman and Tasdemir [69], Blanco et al. [70], and Demirboga [71] also reported that the TC decreased due to the decreasing of concrete density. Lu-Shu et al. [72] stated that the TC increased with increasing density by giving a relation, experimentally formulated, between the density and TC. The decreases in the TC of concrete may be also due to the internal crack growth and deterioration in the microstructure and the increase in porosity of specimens by means of re-expansion of vermiculite during thermal treatment.

SEM Analysis

Dehydration, including the release of chemically bound water from calcium silicate hydrate (C-S-H), becomes significant above 110°C. The dehydration of the matrix and the thermal expansion of the aggregate increase the internal stresses; from 300°C upward, micro-cracks appear through the material. When the temperature exceeds 400°C, C-S-H begins to damage and the strength of the concrete decreases rapidly; the structure of C-S-H disperses at about 900°C [17].

SEM investigations were conducted on air-cooled specimens of all mixtures for each heating temperature (T). The SEM observations are given in Figures 9a to 9e. From the SEM images, changes in the cement paste phase at the heating temperature of 300°C were observed when compared to 20°C, and it may be concluded that a deterioration in microstructure starts at the heating temperature of 300°C. However, there was no additional significant damage in the cement phase up to the heating temperature of 900°C. At 900°C, it may be said that the bond between cement paste and vermiculite aggregate may increase by resulting in some chemical reactions, since increases in strength were observed at those temperatures. At 1,100°C, it is observed that the structure of C-S-H dispersed and bond strength became weak since the transition zone started to disappear. The increase in internal cracking and pore structure coarsening of the specimens at 1,100°C (seen in Figure 9e) is probably responsible for the occurrence of a significant decrease in compressive and splitting tensile strengths.

ANALYSIS RESULTS

In this study, ANN models, namely RBNN and MLP, and the MLR and MNLR models are devised to estimate the TC of concrete containing vermiculite. For this purpose, the TC was chosen as a dependent variable and T, C, P, w, and V were chosen as independent variables. The data presented herein were used in developing these models. Twenty experimental datasets were used. For the training phase, 12 datasets (approximately 60%) were randomly selected, and the remaining 8 datasets (approximately 40%) were selected for testing phase.

MLR and MNLR were performed for the 12 experimental datasets and tested using the remaning 8 datasets. The obtained MLR and MNLR equations are as follows:

$$TC = 0.4956 - 0.0002 \times T + 0.0003 \times C - 0.0009 \times w + 0.0009 \times V, \quad (9)$$

$$TC = 2.993 \times 10^{-7} \frac{C^{1.312} \times w^{0.423} \times V^{1.667}}{T^{0.196} \times P^{1.372}}. \quad (10)$$

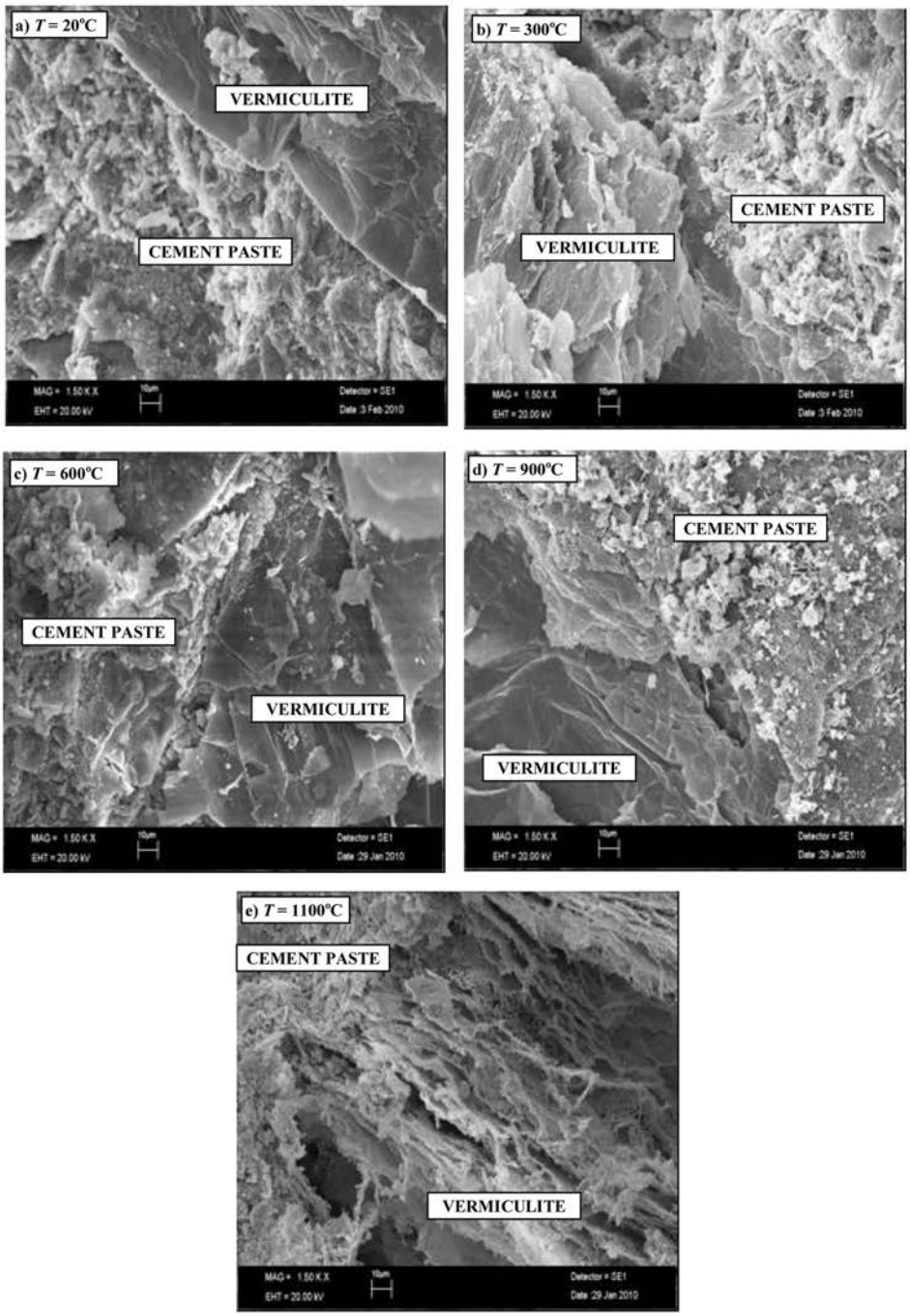

Figure 9. SEM analysis: (a) $T = 20°C$, (b) $T = 300°C$, (c) $T = 600°C$, (d) $T = 900°C$, and (e) $T = 1{,}100°C$.

Before applying the ANN to the data, the training input and output values were normalized using the equation

$$a\frac{x_i - x_{\min}}{x_{\max} - x_{\min}} + b, \tag{11}$$

where $x_{\min}$ and $x_{\max}$ denote the minimum and maximum of the training and test data, respectively. Different values can be assigned for scaling factors a and b. There are no fixed rules as to which standardization approach should be used in particular circumstances [73]. A range of 0.2–0.8 increases the extrapolation ability of the ANN models [74–76]. Therefore, in this study, a and b were taken as 0.6 and 0.2, respectively.

Two different ANN models, namely RBNN and MLP, were developed to improve MLR and MNLR results in estimation of the TC of concrete. For this purpose, two different program codes, including neural networks, were written in MATLAB language. Different ANN architectures were tried using these codes, and the appropriate model structures were determined. Different numbers of hidden neurons and spread constants were examined for the RBNN models. The optimum hidden-layer neuron number and spread constant value that give the minimum root mean square errors (RMSEs) were found to be 3 and 1.2, respectively. The best MLP results were obtained for three neurons in the hidden layer using the logarithmic sigmoid and linear activation functions for the hidden- and output-layer neurons, respectively.

The RMSE, mean absolute error (MAE), and determination coefficient (R^2) values of RBNN, MLP, MLR, and MNLR for both training and testing phases are given in Table 5. The RMSE and MAE shown in Table 5 are defined as follows:

$$RMSE = \sqrt{\frac{1}{N}\sum_{i=1}^{N}[(TC)_{i_{measured}} - (TC)_{i_{predicted}}]^2}, \tag{12}$$

$$MAE = \frac{1}{N}\sum_{i=1}^{N}|(TC)_{i_{measured}} - (TC)_{i_{predicted}}|, \tag{13}$$

in which N is the number of datasets.

The ANN models were then tested, and the results were compared by means of RMSE, MAE, and R^2 statistics, as shown in Table 5. As seen from Table 5, although the MLP model has the smallest RMSE (0.005) and MAE (0.0039) and the highest R^2 (0.998) for the training phase, the RBNN model has the smallest RMSE (0.013), MAE (0.011), and R^2 (0.991) for testing phase. According to the test results, the RBNN and MLP

Table 5. RMSE, MAE, and R^2 statistics of RBNN, MLP, MNLR, and MLR models

	Training			Testing		
Method	RMSE	MAE	R^2	RMSE	MAE	R^2
RBNN	0.006	0.005	0.997	0.013	0.011	0.991
MLP	0.005	0.004	0.998	0.014	0.011	0.988
MNLR	0.027	0.024	0.939	0.027	0.019	0.922
MLR	0.059	0.047	0.786	0.045	0.027	0.805

Table 6. Test results and calculated TCs by RBNN, MLP, MNLR, and MLR models

Number of tests	TC					ARE (%)			
	Observed	RBNN	MLP	MNLR	MLR	RBNN	MLP	MNLR	MLR
1	0.37	0.35	0.37	0.31	0.37	7.1	1	15.8	0.8
2	0.22	0.23	0.22	0.25	0.25	5.9	3.4	15.2	15.6
3	0.47	0.46	0.45	0.48	0.36	1.8	2.8	3.4	23.3
4	0.22	0.22	0.21	0.25	0.24	1.6	3.9	13.5	10.9
5	0.14	0.15	0.15	0.19	0.13	8.1	4.3	32.9	7.7
6	0.17	0.17	0.15	0.18	0.09	2.6	11.2	6.1	46.7
7	0.33	0.32	0.30	0.30	0.27	3	8.5	7.9	18.5
8	0.14	0.14	0.15	0.17	0.15	6.5	1.2	6.1	4.1

models provide RMSE, MAE, and R^2 values close to each other. The RBNN estimations are slightly better than those of the MLP, and these two produced more accurate results than the MNLR and MLR.

The observed TC values and those predicted by RBNN, MLP, MNLR, and MLR models are given in Table 6. The absolute relative errors (AREs) for RBNN, MLP, MNLR, and MLR models are also presented in Table 6. The ARE of model prediction was used as the accuracy of the models.

The ARE is defined as

$$ARE(\%) = \left| \frac{TC_{observed} - TC_{predicted}}{TC_{observed}} \right| \times 100. \tag{14}$$

Observed TC values and estimates by the RBNN, MLP, MNLR, and MLR models are shown in Figure 10. It can be seen from Figure 10 that the MNLR and MLR performances are unsatisfactory in the prediction of TC values in comparison with the RBNN and MLP models. The RBNN and MLP models seem to have similar accuracy, and both are significantly superior to the MNLR and MLR models.

GENERAL DISCUSSION AND CONCLUSION

The developed high-temperature heat-insulating cement-based materials produced by using expanded vermiculite can be used in thermal power plants with the hot-wall temperature as an alternative to lightweight chamotte components and fibrous heat insulators. Since the V/C ratio and heating temperature are the two significant parameters influencing the TC of cement-based composites, results of the TC as a function of these parameters were compiled. TC decreased by increasing expanded vermiculite in the mix and heating up to the temperature of 900°C. The TC for V/C ratios of 3, 4, 5, and 6 was observed to be lower when compared to the unheated control specimens as 58.4%, 60.1%, 63.7%, and 63.6%, respectively. The significant degradations and damages in the microstructure of concrete produced by using expanded vermiculite occur above the temperature of 900°C. It is observed that the critical exposure temperature for loss of compressive strengths is above 900°C.

The development of a model based on existing experimental data becomes necessary to predict material properties. It may significantly reduce further experimental work in

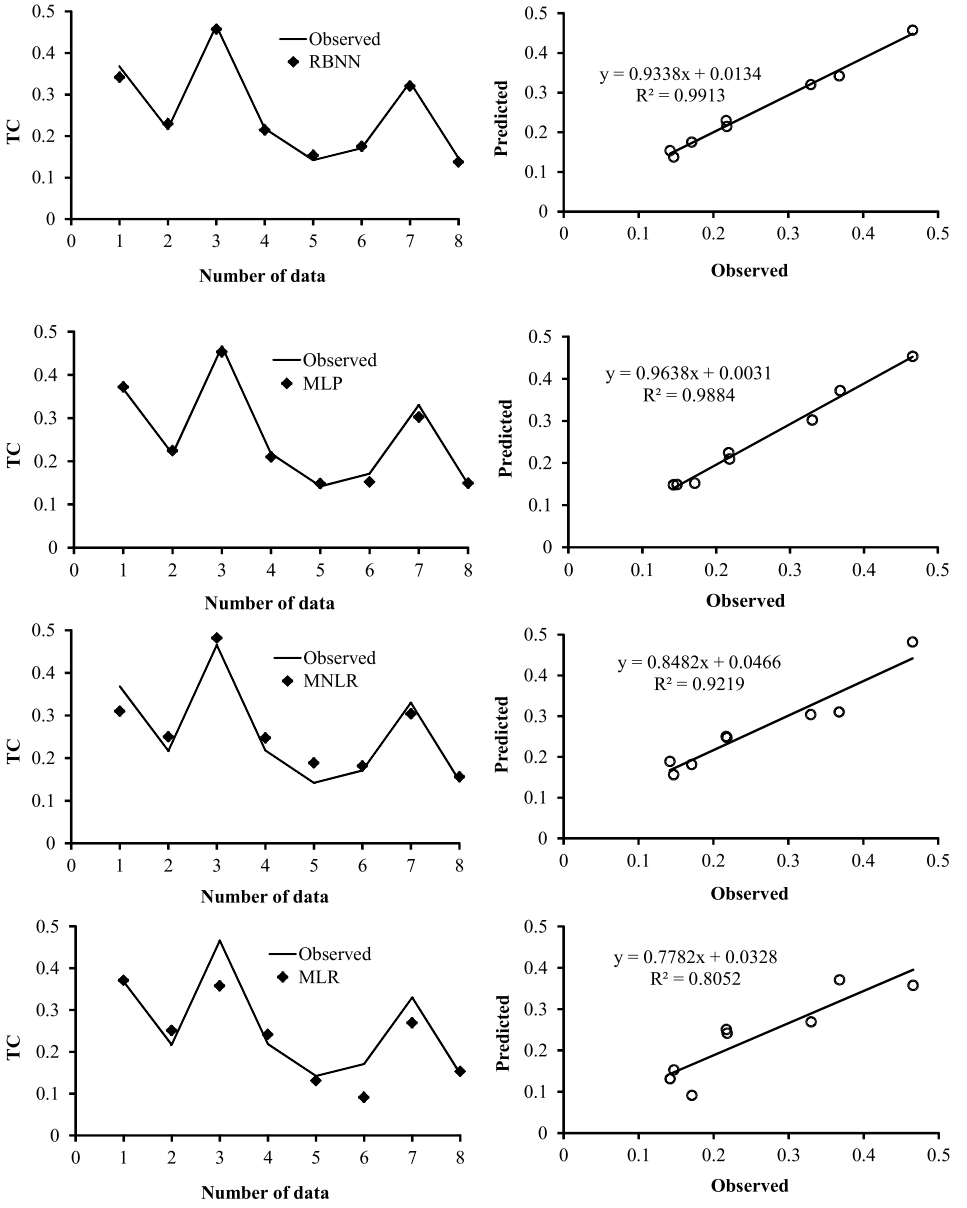

Figure 10. Plot of observed and predicted TC using by RBNN, MLP, MNLR, and MLR.

the design of composite materials. Simulation of material properties generally involves the development of a mathematical model derived from experimental data; it is helpful in the materials optimization, especially for composites like concrete. For this purpose, the ANN has been introduced into this field in recent years and successfully applied in a number of diverse fields, including engineering problems, since the above-mentioned model approaches seem to have good potential to save time and cut expenses in solving various engineering problems.

This article evaluates RBNN and MLP approaches for determining the TCs of concrete. For this purpose, experimental studies were conducted to investigate the influence temperature, cement, porosity, vermiculite, and water on TCs of concrete, and models are developed to predict TCs of concrete. In these models, 20 datasets are used. For the training set, 12 datasets (60%) were randomly selected, and the residual datasets (8 datasets, 40%) were selected as the test set. Results of experimental studies were used to compare with those obtained by the RBNN, MLP, MNLR, and MLR approaches. To verify the models, regression equations are carried out and compared with the trained RBNN, MLP, MNLR, and MLR. The high value of R^2 and low value of RMSE and MAE of the testing set indicated that the RBNN can be used for the prediction of the TC of concrete. By the statistics of the effect of variables on the test results based on MNLR and MLR models, vermiculite was the most influential variable on the TC. This study has indicated that the RBNN model is the best predictor of TC between four models because of the best value of RMSE, MAE, and R^2 statistics and can be employed successfully in estimation of TC for concrete. The results indicate that the developed models are reliable, accurate, and result in good agreement with the experimental studies. The study showed that within the range of input parameters being investigated, the results of the RBNN show consistency and accuracy when compared to the results as given by others. Thus, the present study suggests that the RBNN is an alternative approach for TC assessment of concrete against other prediction methods.

Cement-based material produced by expanded vermiculite can be used as a new material and structural component with good physical material properties for housing and other structures. In order to develop or increase the performance of similar materials in the future, mix proportion may be optimized by taking into account different mix proportions and curing conditions. Also, polymer-based lightweight concretes using expanded vermiculite may be produced as an alternative to cement-based one. Finally, composites to be produced with expanded vermiculite may become a viable and promising construction material for the point of view of energy conscious and ecological design in future.

ACKNOWLEDGMENT

The authors would like to thank The Higher Education Council of Turkey in Ankara for financial support.

REFERENCES

1. O. Sengul, S. Azizi, F. Karaosmanoglu, and M. A. Tasdemir, Effect of Expanded Perlite on the Mechanical Properties and Thermal Conductivity of Lightweight Concrete, *Energy Build.*, vol. 43, pp. 671–676, 2011.

2. J. Xaman, G. Mejia, G. Alvarez, and Y. Chavez, Analysis on the Heat Transfer in a Square Cavity with a Semitransparent Wall: Effect of The Roof Materials, *Int. J. Therm. Sci.*, vol. 49, pp. 1920–1932, 2010.
3. ACI Committee 122, *Guide to Thermal Properties of Concrete and Masonry Systems*, ACI 122R-02, Detroit, p. 21, 2002.
4. K. Arendt, M. Krzaczek, and J. Florczuk, Numerical Analysis by FEM and Analytical Study of the Dynamic Thermal Behavior of Hollow Bricks with Different Cavity Concentration, *Int. J. Therm. Sci.*, vol. 50, pp. 1543–1553, 2011.
5. A. M. Papadopoulous and E. Giama, Environmental Performance Evaluation of Thermal Insulation Materials and Its Impact on the Building, *Build. Environ.*, vol. 42, pp. 2178–2187, 2007.
6. F. Mathieu-Potvin and L. Gosselin, Thermal Shielding of Multilayer Walls with Phase Change Materials under Different Transient Boundary Conditions, *Int. J. Therm. Sci.*, vol. 48, pp. 1707–1717, 2009.
7. B. Yesilata, H. Bulut, and P. Turgut, Experimental Study on Thermal Behavior of a Building Structure Using Rubberized Exterior Walls, *Energy Build.*, vol. 43, pp. 393–399, 2011.
8. A. Hasan, Optimising Insulation Thickness for Buildings Using Life Cycle Cost, *Appl. Energy*, vol. 63, pp. 115–124, 1999.
9. R. Demirboga, Thermal Conductivity and Compressive Strength of Concrete Incorporation with Mineral Admixtures, *Build. Environ.*, vol. 42, pp. 2467–2471, 2007.
10. X. Q. Li, Y. Chen, J. D. Spitler, and D. Fisher, Applicability of Calculation Methods for Conduction Transfer Function of Building Constructions, *Int. J. Therm. Sci.*, vol. 48, pp. 1441–1451, 2009.
11. J. J. del Coz Díaz, P. J. García Nieto, L. M. Díaz Pérez, and P. Riesgo Fernández, Nonlinear Thermal Analysis of Multi-Holed Lightweight Concrete Blocks Used In External and Non Habitable Floors by FEM, *Int. J. Heat Mass Tranf.*, vol. 54, pp. 533–548, 2011.
12. J. J. del Coz Díaz, P. J. García Nieto, J. Domínguez Hernández, and F. P. Álvarez Rabanal, A FEM Comparative Analysis of The Thermal Efficiency Among Floors Made Up of Clay, Concrete and Lightweight Concrete Hollow Blocks, *Appl. Thermal Eng.*, vol. 30, pp. 2822–2826, 2010.
13. J. J. del Coz Díaz, P. J. García Nieto, J. Domínguez Hernández, and A. Suárez Sánchez, Thermal Design Optimization of Lightweight Concrete Blocks for Internal One-Way Spanning Slabs Floors by FEM, *Energy Build.*, vol. 41, pp. 1276–1287, 2009.
14. J. J. del Coz Díaz, P. J. García Nieto, J. L. Suárez Sierra, and I. Peñuelas Sánchez, Non-Linear Thermal Optimization and Design Improvement of a New Internal Light Concrete Multi-Holed Brick Walls by FEM, *Appl. Thermal Eng.*, vol. 28, pp. 1090–1100, 2008.
15. J. J. del Coz Díaz, P. J. García Nieto, J. L. Suárez Sierra, and C. Betegón Biempica, Nonlinear Thermal Optimization of External Light Concrete Multi-Holed Brick Walls by The Finite Element Method, *Int. J. Heat Mass Tranf.*, vol. 51, pp. 1530–1541, 2008.
16. M. I. Khan, Factors Affecting the Thermal Properties of Concrete and Applicability of Its Prediction Models, *Build. Environ.*, vol. 37, pp. 607–614, 2002.
17. O. Gencel, Effect of Elevated Temperatures on Mechanical Properties of High Strength Concrete Containing Varying Proportions of Hematite, *Fire Materials*, vol. 36, pp. 217–230, 2011.
18. Y. Xu and D. D. L. Chung, Improving Silica Fume by Using Silane, *Cem. Concr. Res.*, vol. 30, pp. 1305–1311, 2000.
19. O. Sengul, C. Tasdemir, and M. A. Tasdemir, Influence of Aggregate Type on the Mechanical Behaviour of Normal and High Strength Concretes, *ACI Mater. J.*, vol. 99, pp. 528–533, 2002.
20. G. M. Glenn, A. K. Klamczynski, B. S. Chiou, D. Wood, W. J. Orts, and S. H. Imam, Lightweight Concrete Containing an Alkaline Resistant Starch-Based Aquagel, *J. Polym. Environ.*, vol. 12, pp. 189–196, 2004.

21. K. S. Al-Jabri, A. W. Hago, R. Taha, A. S. Alnuaimi, and A. H. Al-Saidy, Strength and Insulating Properties of Building Blocks Made from Waste Materials, *J. Mater. Civil Eng.*, vol. 21, pp. 191–197, 2009.
22. S. Dermirdag and L. Gunduz, Strength properties of Volcanic Slag Aggregate Lightweight Concrete for High Performance Masonry Units, *Constr. Build. Mater.*, vol. 22, pp. 135–142, 2008.
23. J. Addisson, Vermiculite: A Review of the Mineralogy and Health Effects of Vermiculite Exploitation, *Regul. Toxicol. Pharm.*, vol. 21, pp. 397–405, 1996.
24. W. A. Deer, R. A. Howie, and J. Zussman, *Rock-Forming Minerals, Sheet Silicates*, 2nd ed., Longman, London, chap. 3, 1963.
25. C. D. L. Calla and H. Suquet, Vermiculite: In Hydrous Phyllosilicates (Exclusive of Micas), in S. W. Bailey (Ed.), *Reviews in Mineralogy 19*, Mineralogical Society of America, Washington, DC, pp. 455–496, 1988.
26. P. B. Malla, Vermiculites–Chemistry, Mineralogy, and Applications, in J. B. Dixon and D. G. Schulze (Eds.), *Soil Mineralogy with Environmental Applications, SSSA Series No. 7*, Soil Science Society of America, pp. 501–529, 2002.
27. S. A. Suvorov and V. V. Skurikhin, Vermiculite—A Promising Material for High-Temperature Heat Insulators, *Refract. Ind. Ceram.*, vol. 44, pp. 186–193, 2003.
28. D. G. Schulze, An Introduction to Soil Mineralogy, in J. B. Dixon and D. G. Schulze (Eds.), *Soil Mineralogy with Environmental Applications, SSSA Series No. 7*, Soil Science Society of America, pp. 1–35, 2002.
29. O. Gencel, F. Kocabas, M. S. Gok, and F. Koksal, Comparison of Artificial Neural Networks and General Linear Model Approaches for The Analysis of Abrasive Wear of Concrete, *Constr. Build. Mater.*, vol. 25, pp. 3486–3494, 2011.
30. I. C. Yeh, Design of High-Performance Concrete Mixture Using Neural Networks and Nonlinear Programming, *J. Comput. Civil Eng.*, vol. 13, pp. 36–42, 1999.
31. J. W. Oh, Application of Neural Networks for Proportioning of Concrete Mixes, *ACI Mater. J.*, vol. 96, pp. 61–67, 1999.
32. T. A. Ji, Mortar Mix Proportion Design Algorithm Based on Artificial Neural Networks, *Comput. Concr.*, vol. 3, pp. 357–373, 2006.
33. T. Ji, T. Lin, and X. Lin, A Concrete Mix Proportion Design Algorithm Based on Artificial Neural Networks, *Cem. Concr. Res.*, vol. 36, pp. 1399–1408, 2006.
34. A. Oztas, M. Pala, E. Ozbay, E. Kanca, N. Caglar, and M. A. Bhatti, Predicting the Compressive Strength and Slump of High Strength Concrete Using Neural Network, *Constr. Build. Mater.*, vol. 20, pp. 769–775, 2006.
35. I. C. Yeh, Modeling Slump Flow of Concrete Using Second-Order Regressions and Artificial Neural Networks, *Cem. Concr. Compos.*, vol. 29, pp. 474–480, 2007.
36. I. C. Yeh, Modeling Slump of Concrete with Fly Ash and Superplasticizer, *Comput. Concr.*, vol. 5, pp. 559–572, 2008.
37. I. C. Yeh, Prediction of Workability of Concrete Using Design of Experiments for Mixtures, *Comput. Concr.*, vol. 5, pp. 1–20, 2008.
38. M. Bilgehan and P. Turgut, Artificial Neural Network Approach to Predict Compressive Strength of Concrete Through Ultrasonic Pulse Velocity, *Res. Nondestr. Eval.*, vol. 21, pp. 1–17, 2010.
39. M. Bilgehan and P. Turgut, The Use of Neural Networks in Concrete Compressive Strength Estimation, *Comput. Concr.*, vol. 7, pp. 271–283, 2010.
40. S. C. Lee, Prediction of Concrete Strength Using Artificial Neural Networks, *Eng. Struct.*, vol. 25, pp. 849–857, 2003.
41. A. Mukherjee and S. N. Biswas, Artificial Neural Networks in Prediction of Mechanical Behavior of Concrete at High Temperature, *Nucl. Eng. Des.*, vol. 178, pp. 1–11, 1997.

42. I. B. Topcu and M. Saridemir, Prediction of Properties of Waste AAC Aggregate Concrete Using Neural Network, *Comput. Mat. Sci.*, vol. 41, pp. 117–125, 2007.
43. H. Erdem, Prediction of the Moment Capacity of Reinforced Concrete Slabs in Fire Using Artificial Neural Networks, *Adv. Eng. Softw.*, vol. 41, pp. 270–276, 2010.
44. European Standards, *Cement. Part 1: Compositions and Conformity Criteria for Common Cements*, European norm EN 197-1/A1, Ankara, Turkey, 2005.
45. American Society for Testing and Materials (ASTM), *Standard Test Method for Compressive Strength of Cylindrical Concrete Specimens*, Annual Book of ASTM Standards, ASTM C39, Pennsylvania, 2009.
46. American Society for Testing and Materials (ASTM), *Standard Test Method for Thermal Conductivity of Refractories by Hot Wire Platinum Resistance Thermometer Technique*, ASTM C1113-99, 2004.
47. W. R. Daire and A. Downs, The Hot Wire Test—A Critical Review and Comparison with B 1902 Panel Test, *Trans. Brit. Ceramic Soc.*, vol. 79, p. 44, 1980.
48. J. C. Willshee, Comparison of Thermal Conductivity Methods, *Proc. Brit. Ceramic Soc.*, vol. 29, p. 153, 1980.
49. K. Sengupta, R. Das, and G. Banerjee, Measurement of Thermal Conductivity of Refractory Bricks by the Nonsteady State Hot-Wire Method Using Differential Platinum Resistance Thermometry, *J. Test. Eval.*, vol. 29, pp. 455–459, 1992.
50. S. Haykin, *Neural Networks: A Comprehensive Foundation*, 2nd ed., Prentice-Hall, Upper Saddle River, NJ, 1998.
51. D. S. Broomhead and D. Lowe, Multi-Variable Functional Interpolation and Adaptive Networks, *Complex Syst.*, vol. 2, pp. 321–355, 1988.
52. T. Poggio and F. Girosi, Regularization Algorithms for Learning That are Equivalent to Multilayer Networks, *Science*, vol. 2247, pp. 978–982, 1990.
53. J. A. Leonard, M. A. Kramer, and L. H. Unga, Using Radial Basis Functions to Approximate a Function and Its Error Bounds, *IEEE T. Neural Network*, vol. 3, pp. 624–627, 1992.
54. G. C. Lee and S. H. Chang, Radial Basis Function Networks Applied to DNBR Calculation in Digital Core Protection Systems, *Ann. Nucl. Energy*, vol. 30, pp. 1561–1572, 2003.
55. L. Fausett, *Fundamentals of Neural Networks*, Prentice Hall, Englewood Cliffs, NJ, 1994.
56. O. Kisi, The Potential of Different ANN Techniques in Evapotranspiration Modeling, *Hydrol. Process.*, vol. 22, pp. 2449–2460, 2008.
57. F. Kocabas and S. Unal, Compared Techniques for the Critical Submergence of an Intake in Water Flow, *Adv. Eng. Softw.*, vol. 41, pp. 802–809, 2010.
58. H. K. Cigizoglu and O. Kisi, Flow Prediction by Three Backpropagation Techniques Using K-Fold Partitioning of Neural Network Training Data, *Nordic Hydrol.*, vol. 36, pp. 49–64, 2005.
59. M. T. Hagan and M. Menhaj, Training Feedforward Networks with the Marquardt Algorithm, *IEEE T. Neural Network*, vol. 5, pp. 989–993, 1994.
60. F. Kocabas, O. Kisi, and M. Ardıclioglu, An Artificial Neural Network Model for Prediction of Critical Submergence for an Intake in a Stratified Fluid Media, *Civil Eng. Environ. Syst.*, vol. 26, pp. 367–375, 2009.
61. G. Cybenco, Approximation by Superposition of a Sigmoidal Function, *Math. Control Signals Syst.*, vol. 2, pp. 303–314, 1989.
62. K. Hornik, M. Stinchcombe, and H. White, Multilayer Feed Forward Networks are Universal Approximators, *Neural Networks*, vol. 2, pp. 359–366, 1989.
63. E. Pinar, K. Paydas, G. Seckin, H. Akilli, B. Sahin, M. Cobaner, S. Kocaman, and M. A. Akar, Artificial Neural Network Approaches for Prediction of Backwater Through Arched Bridge Constrictions, *Adv. Eng. Softw.*, vol. 41, pp. 627–635, 2010.
64. J. J. More, The Levenberg–Marquardt Algorithm: Implementation and Theory, in G. A. Watson (Ed.), *Numerical Analysis, Lecture Notes in Mathematics, vol. 630*, Springer Verlag, Berlin, pp. 105–116, 1997.

65. O. Kisi and H. K. Cigizoglu, Comparison of Different ANN Techniques in River Flow Prediction, *Civil Eng. Environ. Syst.*, vol. 14, pp. 211–231, 2007.
66. F. Kocabas, S. Unal, and B. Unal, A Neural Network Approach for Prediction of Critical Submergence of an Intake in Still Water and Open Channel Flow for Permeable and Impermeable Bottom, *Comput. Fluids*, vol. 37, pp. 1040–1046, 2008.
67. O. Gencel, The Application of Artificial Neural Networks Technique to Estimate Mass Attenuation Coefficient of Shielding Barrier, *Int. J. Phys. Sci.*, vol. 4, pp. 743–751. 2009.
68. O. Kisi, Stream Flow Forecasting Using Different Artificial Neural Network Algorithms, *J. Hydrol. Eng.*, vol. 12, pp. 532–539, 2007.
69. M. S. Akman and M. A. Tasdemir, Perlite Concrete as a Structural Material, *First National Perlite Congress*, Ankara, Turkey, December 20–22, 1977 (in Turkish).
70. F. Blanco, P. Garcia, P. Mateos, and J. Ayala, Characteristics and Properties of Lightweight Concrete Manufactured with Cenospheres, *Cem. Concr. Res.*, vol. 30, pp. 1715–1722, 2000.
71. R. Demirboga, Influence of Mineral Admixtures on Thermal Conductivity and Compressive Strength of Mortar, *Energy Build.*, vol. 35, pp. 189–192, 2003.
72. K. Lu-Shu, S. Man-Qing, S. Xing-Sheng, and L. Yun-Xiu, Research on Several Physico Mechanical Properties of Lightweight Aggregate Concrete, *Int. J. Lightweight Concrete*, vol. 2, pp. 185–191, 1980.
73. O. Kisi, Daily Pan Evaporation Modelling Using Multi-Layer Perceptrons and Radial Basis Neural Networks, *Hydrol. Process.*, vol. 23, pp. 213–223, 2008.
74. O. Kisi and M. Cobaner, Modeling River Stage-Discharge Relationships Using Different Neural Network Computing Techniques, *Clean-Soil-Air-Water*, vol. 37, pp. 160–169, 2009.
75. H. K. Cigizoglu, Estimation, Forecasting and Extrapolation of River Flows by Artificial Neural Networks, *Hydrol. Sci. J.*, vol. 48, pp. 349–361, 2003.
76. O. P. Modi, D. P. Mondal, B. K. Prasad, M. Singh, and H. K. Khaira, Abrasive Wear Behavior of High Carbon Steel: Effects of Microstructure and Experimental Parameters and Correlation with Mechanical Properties, *Mater. Sci. Eng. A*, vol. 343, pp. 235–242, 2003.